

Malaysian Journal of Mathematical Sciences

Journal homepage: https://mjms.upm.edu.my



Electrical MHD Flow via Stretching Sheet with Arrhenius Activation Energy utilizing Modified Buongiorno Model: The Optimization

Norzawary, N. H. A.* ¹⁰¹, Bakar, S. A. ¹⁰², Pop, I. ¹⁰³, Wahid, N. S. ¹⁰⁴, Arifin, N. M. ^{101,4}, and Bachok, N. ^{101,4}

¹Institute for Mathematical Research, Universiti Putra Malaysia,
43400 Serdang, Malaysia

²Takasago Thermal/Environmental System Laboratory,
Malaysia-Japan International Institute of Technology, Universiti Teknologi Malaysia,
54100 Kuala Lumpur, Malaysia

³Department of Mathematics, Babes-Bolyai University, R-400084, Cluj-Napoca, Romania

⁴Department of Mathematics and Statistics, Faculty of Science, Universiti Putra Malaysia,
43400 Serdang, Malaysia

E-mail: nurhazirah.adilla@gmail.com *Corresponding author

Received: 20 December 2024 Accepted: 13 April 2025

Abstract

This research highlights a comprehensive mathematical model of Arrhenius activation energy and viscous dissipation impacts on electrically conductive magnetohydrodynamic (MHD) flow via shrinking sheet. The model utilizes a modified Buongiorno approach, which implies nano fluid dynamics factors such as thermophoresis and Brownian motion. In general description, electrical MHD describes fluid flow such as plasma or liquid metals that influenced by electric and magnetic fields. The Arrhenius activation energy effect then introduces a temperaturedependent reaction rate that typically modelled by an exponential function, considering its ability in increasing reaction rates as temperature rises. The mathematical derivation of this study involves a transformation of partial differential equations converting to ordinary differential equations, subjected to their respective boundary conditions, through a similarity transformation to simplifies complex interactions into a solvable framework. These equations are numerically solved employing byp4c function in MATLAB to observe precise analysis of flow behaviour and heat transfer properties. The study conclude that the magnetic parameter and Brownian motion parameter reduce heat transfer, while the activation energy and temperature difference parameters amplify concentration profiles. The inclusion of the electric field parameter is shown to elevate the boundary layer flow and heat transfer rate. Based on the heat transfer analysis, an optimization by Response Surface Methodology (RSM) further analyses these solutions to identify an optimal combination of three critical parameters in order to maximize heat transfer rate. This optimization provides insights in efficient thermal management applications and supports advancements in cooling or energy sustainability.

Keywords: electrical MHD; Arrhenius activation energy; modified Buongiorno model; response surface methodology; stretching.

1 Introduction

The optimization of heat transfer in MHD flows is an important area of research due to its applications in space technology, renewable energy systems, as well as biomedical devices. The use of nanofluids—suspensions of nanoparticles in base fluids—has significantly enhances thermal conductivity and making them an important subject for detailed study. The modified Buongiorno model then provides a robust framework in analysing nanofluid dynamics in light of the implications of Brownian motion and thermophoresis. The original Buongiorno model, which introduced by Buongiorno [9], considered nanofluids as a two-phase system. This model accounts for the relative movement of nanoparticles and the base fluid, specifically addressing thermophoresis (the motion of particles due to temperature gradients) and Brownian diffusion (random particles movement within fluid). It provides a theoretical basis to understand how nanoparticles influence heat and mass transfer processes.

Researchers such as Turkyilmazoglu [50] used the Buongiorno model to analyse nanofluid flow in an asymmetric channel, showing that the integrated impacts of thermophoresis and Brownian motion can enhance the Nusselt number, increasing heat transfer while reducing the fluid temperature. Anwar [5] then extended this work by studying transport phenomena and frictional relaxation times in nanofluid flow using the Buongiorno model, confirming that Brownian motion and thermophoresis parameters increase temperature profiles while reducing concentration profiles. Further research by Rawat et al. [41] observed mixed convection nanofluid flow in a cone and wedge with chemical reactions and thermal radiation. Their analysis found that the Brownian motion parameter does not affect temperature under zero mass flux conditions at the wall, whereas the thermophoresis parameter increases the temperature distribution. Chu et al. [11] executed a numerical study of nanofluid flow via stretching disk with gyrotactic microorganisms, revealing that Brownian motion decreases concentration profiles while thermophoresis increases temperature profiles.

In the meantime, Owhaib et al. [36] justified that the thermal layer structure improved with Brownian motion parameter as stated in their study of nanofluid flow via three-dimensional rotating sheet with viscous heating and radiation parameters. Gurrampati and Vijaya [19] then performed on MHD Casson nanofluid flow via inclined porous sheet employing Buongiorno model. The development of the modified Buongiorno model involves integrating additional terms into the governing equations to account for these physical phenomena. These equations are then solved under various boundary conditions to simulate practical scenarios. Researchers have applied the model to study diverse flow conditions and geometries, including flat plates [10], stretching or shrinking surfaces [40], wavy channels [13], and rotating disks [3].

Additionally, Arrhenius activation energy is the minimum energy essential for a chemical reaction to emerge. For example, in catalytic nanofluids, such as the decomposition of hydrogen peroxide with nanoparticles, the reaction rate increases with temperature as governed by the Arrhenius equation and this makes it central to understanding temperature-dependent reaction rates, as it explains how an increase in temperature accelerates reactions [23]. However, a major drawback of Arrhenius energy is its assumption of a fixed activation energy, which may not suit complex reactions with variable energy barriers. This limitation can be addresses by integrating advanced models like Buongiorno model, or Eyring equation [37]. Such studies on Arrhenius activation energy have been extensively explored in various contexts.

Khan et al. [24] analysed the second law of thermodynamics in nanofluid flow alongside binary chemical reactions and Arrhenius activation energy, finding that the activation energy parameter reduced the nanofluid's concentration profiles. Ramzan et al. [39] later examined its impact

on 3D bioconvection nanofluid flow with ion slip and Hall current, while Bhatti and Michaelides [7] studied thermos-bioconvection nanofluid flow via Riga plate incorporating Arrhenius activation energy. In a study of a Casson nanofluid flow via deformable cylinder employing Soret Dufour effects, Arrhenius activation energy, and variable characteristics that was developed by Shaheen et al. [45], they confirmed that activation energy parameter improves the concentration distribution. Further, Jayaprakash et al. [22] reported that this parameter reduced the rate of mass transfer but increased chemical reaction profiles in their study on convective heat transfer effectiveness in hybrid nanofluid flow with radiation and Arrhenius activation energy. Additional insights into related studies can be found in Sharma et al. [48] who investigated the impact of Arrhenius activation energy on MHD nanofluid flow using a modified Buongiorno model, and Zahir et al. [51] who analyzed entropy generation and activation energy effects in the peristaltic transport of Prandtl-Eyring fluids.

Magnetohydrodynamic (MHD) flows and heat transfer involving Jeffrey fluids are widely studied for their engineering applications. Research highlights the effects of viscous dissipation, non-isothermal conditions, and particle-fluid interactions on flow and heat transfer over stretching sheets [2]. Meanwhile, studies by Kumar et al. [27] on velocity slip conditions in MHD peristaltic flows of Prandtl fluids show how factors like the velocity slip and Hartmann number influence pressure and friction in non-uniform channels. Recent work by Norzawary et al. [35] on MHD flow of hybrid carbon nanotubes over a stretching or shrinking sheet with slip further demonstrate enhanced heat transfer efficiency. While MHD focuses on electrically conductive fluids in magnetic fields, electrical MHD adds electric fields, emphasizing the role of electric currents in flow and heat transfer, which adds complexity to these systems.

Another factor in this research is electrical MHD, where it studies the motion of electrically conductive fluids, namely liquid metals, electrolytes, and plasmas, under the influence of electric and magnetic fields [14]. It plays a significant role in fluid dynamics studies by controlling and optimizing flow behaviours in applications where electromagnetic forces dominate over inertial or viscous forces. For instance, electrical MHD can drive fluid flow in small channels using Lorentz force, which enabling precise manipulation or electrolytes in lab-on-a-chip devices for medical diagnostics [18, 47]. The biggest advantage of electrical MHD is its ability to generate flow without moving mechanical parts and this leads to quieter, and more reliable controllable fluid systems. As such, electrical MHD works well with Buongiorno model, which being our key anticipation of this research, as both systems can analyse nanoscale phenomena for instance thermophoresis and Brownian motion. This synergy able to improves the design and efficiency of advanced thermal and chemical systems.

Jagadha et al. [21] studied nanofluid flow with electrical MHD, Soret, Dufour effects, and chemical reactions. They concluded that the electrical MHD parameter enhances temperature profiles while reducing the impact of the convection parameter. Shah et al. [44] then investigated nanofluid flow over rotating porous plates, considering electrical MHD, Joule dissipation, and Hall current, where they highlighted that both temperature profiles and the skin friction coefficient enhance with the electrical MHD parameter. In a study of hybrid nanofluid flow with electrical MHD and partial slip by Gireesha et al. [17], they showed that the electrical field parameter boosts flow velocity, which helps reduce stickiness in hybrid nanofluid flow. In addition, Sharma et al. [49] confirmed that a stronger electric field increases the viscosity of the fluid, although other parameters tend to slow down the fluid movement. Several other researchers such as Gandhi et al. [15], Abrar and Kosar [1] and Razzaq et al. [42] have also examined electrical MHD parameters, demonstrating their significant impact on flow systems.

Further, this study employs a statistical approach called Response Surface Methodology (RSM) to optimize and scrutinize the sensitivity of heat transfer rates. It represents the relationship be-

tween inputs and the response, where RSM uses a combination of experimental design, regression analysis, and optimization techniques to develop an approximate model, often as a polynomial equation. This approach helps identify the optimal combinations for a system of process with minimal experimental efforts [28]. Building on this, other researchers such as Sharifat et al. [46] and Samat et al. [43] have been widely utilized optimization particularly in RSM approach in diverse fluid flow studies. According to the references, this study emphasizes a modified Buongiorno nanofluid model with Arrhenius activation energy and electrical MHD flow via stretching surface. The objectives are defined as follows:

- (a) To develop a mathematical model for the problem.
- (b) To analyze the outcomes of diverse parameters on fluid flow and heat transfer.
- (c) To obtain the ideal arrangement of three parameters to maximize the heat transfer rate.

This study's novelty is based on optimizing thermal conductivity within the modified Buongiorno model, specifically considering Arrhenius activation energy and electrical MHD flow—a combination that has not been previously explored. To formulate the mathematical model, we extended the Partial Differential Equations (PDEs) framework proposed by Daniel et al. [12] to align with our focus. A similarity transformation technique was applied to reform the PDEs into Ordinary Differential Equations (ODEs), which were further resolved employing byp4c program in MATLAB software. The procedure for this function is illustrated in Figure 1.

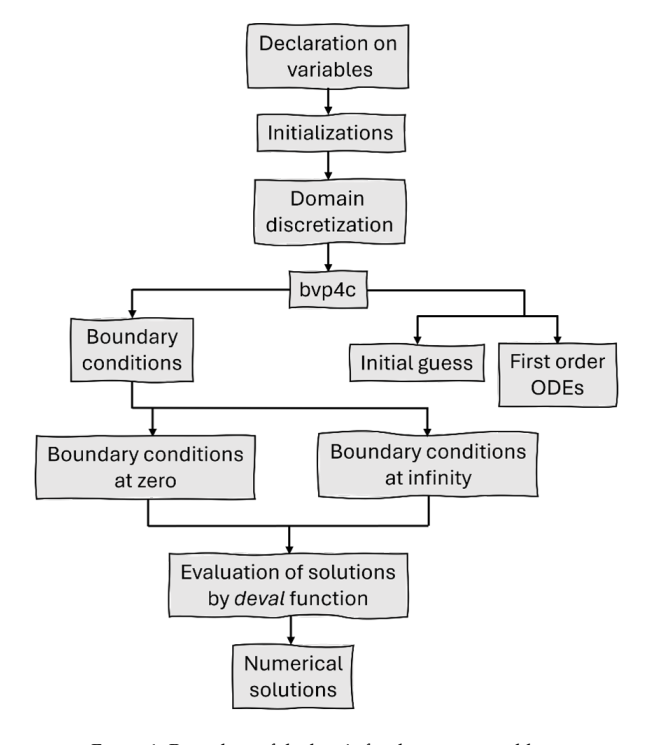


Figure 1: Procedure of the bvp4c for the current problem.

In this study, both numerical and statistical analyses are involved to develop a mathematical model for the current problem and to optimize three selected parameters for enhancing the heat transfer rate. The outcomes of this model are expected to deliver in various applications, including thermal management in electronics, energy-efficient building systems, renewable energy

technologies, advanced cooling systems, industrial heat exchangers, automotive thermal systems, and chemical process optimization [31].

2 Formulation of the Mathematical Model

We examine a steady electrical MHD boundary layer flow, heat transfer, and a concentration of a nanofluid via stretching surface alongside viscous dissipation, Arrhenius activation energy, and Joule heating, as visualized in Figure 2, while the assumption of such model is listed below:

- The system is modeled using Cartesian coordinates, which x-axis aligned across the surface, and the y-axis is perpendicular to it, where the flow takes place for $y \ge 0$.
- The applied magnetic field B_0 , and electric field $E_0(x)$, are directed across the positive *y*-axis.
- The induced magnetic field is neglected due to the low magnetic Reynolds number which means that the applied magnetic field dominates the fluid flow [26].
- The Hall effect is omitted since it primarily influences highly ionized plasmas or rotational flows [25]. In addition, given that our working fluid is a nanofluid with no strong ionization or rotational forces, the Hall parameter remains small, justifying its exclusion.

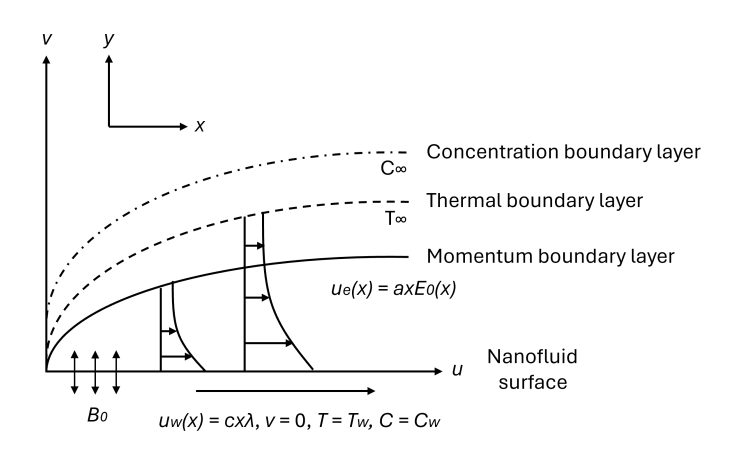


Figure 2: The representation of physical model for current study.

For this study, we utilize Buongiorno nanofluid model [9] which accounts for key nanofluid dynamics such as thermophoresis and Brownian motion effects, which significantly influence heat and mass transfer in nanofluid systems. Unlike conventional nanofluid models that assume uniform nanoparticle distribution, Buongiorno model considers relative velocity between nanoparticles and the base fluid. This model is useful in describing the transport properties of nanofluids, as it accounts for these mechanisms which could significantly improve heat and mass transfer in nanofluid systems [16]. The assumption of this model allows for a more accurate description of how nanoparticles interact with the base fluid affected by thermal and concentration gradients. Based on these hypotheses, the governing equations for the boundary layer flow of this research are the equations of continuity, momentum, energy, and concentration, that formulated in Cartesian coordinates (x,y), which can be written by [12, 38]

$$\frac{\partial u}{\partial x} + \frac{\partial v}{\partial y} = 0,\tag{1}$$

$$u\frac{\partial u}{\partial x} + v\frac{\partial u}{\partial y} = u_e \frac{\partial u_e}{\partial x} + \nu \frac{\partial^2 u}{\partial y^2} + \frac{\sigma B_0}{\rho} [E_0(x) - B_0 u], \tag{2}$$

$$u\frac{\partial T}{\partial x} + v\frac{\partial T}{\partial y} = \alpha \frac{\partial^2 T}{\partial y^2} + \frac{\mu}{\rho C_p} \left(\frac{\partial u}{\partial y}\right) + \frac{\sigma B_0}{\rho} [E_0(x) - B_0 u]^2 +$$

$$\frac{(\rho C_p)_f}{(\rho C_p)_p} \left[D_B \frac{\partial T}{\partial y} \frac{\partial C}{\partial y} + \frac{D_T}{T_\infty} \left(\frac{\partial T}{\partial y} \right)^2 \right],\tag{3}$$

$$u\frac{\partial C}{\partial x} + v\frac{\partial C}{\partial y} = D_B \frac{\partial^2 C}{\partial y^2} + \frac{D_T}{T_\infty} \frac{\partial^2 T}{\partial y^2} + k_r^2 (C - C_\infty) \left(\frac{T}{T_\infty}\right)^m exp\left(-\frac{E_A}{k_1 T}\right),\tag{4}$$

subject to the conditions of,

$$u = u_x(x)\lambda = cx\lambda, \quad v = 0, \quad T = T_w, \quad C = C_w, \quad \text{at} \quad y = 0,$$

$$u \to u_e(x) \to axE_0, \quad T \to T_\infty, \quad C \to C_\infty, \quad \text{as} \quad y \to \infty.$$
 (5)

Here, (u,v) are the velocity components along (x,y)-axes, $u_e(x)=axE_0$ is the velocity of the far field (inviscid flow), and $u_w(x)=cx\lambda$ is the stretching sheet velocity, while E_0 is the strength of the electric field and a, c are constants, with c>0 is for static sheet. Further, $\lambda=\frac{c}{a}>0$ is the constant stretching parameter. The properties of nanofluid as stated in (2) and (3) are α , ρ , ν , μ , ρ , $(C_p)_f$, and $(C_p)_p$, which represented by thermal diffusivity of the fluid, density, kinematic viscosity, electrical conductivity, fluid viscosity, heat capacity of the fluid, and the effective heat capacity of the nanoparticle material, respectively. (T,C), $[T_w(x),C_w]$, and (T_{infty},C_∞) are the temperature and concentration of the nanofluid, surface of the sheet and of the far field, respectively, where $T_w>T_\infty$ and $C_w>C_\infty$. The last term in (4) is then presented as the modified Arrhenius kinetics in which k_r^2 is the reaction rate and k_1 is the Boltzmann constant.

To solve this problem, we propose the following similarity variables [34],

$$u = axf'(\eta), \quad v = -\sqrt{a\nu}f(\eta), \quad \theta(\eta) = \frac{T - T_{\infty}}{\Delta T}, \quad \varphi(\eta) = \frac{C - C_{\infty}}{\Delta C}, \quad \eta = y\sqrt{\frac{a}{\nu}},$$
 (6)

where $\Delta T = T_w - T_\infty$ and $\Delta C = C_w - C_\infty$. To ensure that the Boundary Value Problems (BVPs) in (2)–(4) admit a similarity solution, we presume that $E(x) = xE_1$, where E_1 is a constant, and $T_w(x) - T_\infty = x^2T_0$, where T_0 represents the characteristic surface temperature.

By substituting (6) into the BVPs in (2) to (4), we finally acquire the respective ODEs,

$$f''' + ff'' + \Lambda^2 - (f')^2 + M(\Lambda - f') = 0,$$
(7)

$$\frac{1}{Pr}\theta'' + f\theta' - 2f'\theta + Nb\varphi'\theta' + Nt(\theta')^2 + Ec(f')^2 + M(\Lambda - f')^2 = 0,$$
(8)

$$\varphi'' + Lef\varphi' + \frac{Nt}{Nb}\theta'' + Le\varphi(1+\tau\theta)^m \exp\left(-\frac{A_E}{1+\tau\theta}\right) = 0,$$
(9)

where we observe that the BVPs simplify to forms like those reported by Mahapatra and Gupta [30], Nazar et al. [33], and Bachok et al. [6]. Further, the boundary conditions in (5) can be reduced to,

$$f(0) = 0, \quad f'(0) = \lambda, \quad \theta(0) = 1, \quad \varphi(0) = 1,$$

$$f'(\eta) \to \Lambda, \quad \theta(\eta) \to 0, \quad \varphi(\eta) \to 0, \quad \text{as} \quad \eta \to \infty.$$
 (10)

Based on (7)–(10), the respective parameters are described as follows:

$$M = \frac{\sigma B_0^2}{a\rho}, \quad \Lambda = \frac{E_1}{aB_0}, \quad Nb = \frac{(\rho C_p)_f}{(\rho C_p)_p} \frac{D_B \Delta C}{\nu}, \quad Nt = \frac{(\rho C_p)_f}{(\rho C_p)_p} \frac{D_f \Delta T}{\nu T_\infty},$$

$$Pr = \frac{(\rho C_p)_f}{k_f}, \quad Ec = \frac{c\rho}{C_p \Delta T}, \quad Le = \frac{\nu}{D_B}, \quad A_E = \frac{E_A}{k_1 T_\infty}, \quad \tau = \frac{\Delta T}{T_\infty},$$
(11)

where M, Λ , Nb, and Nt are parameter of magnetic, electric field, Brownian motion and thermophoresis, respectively. Further, Pr, Ec, and Le are the number of Prandt, Eckert and dimensionless Lewis, respectively, and A_E is activation energy parameter, with τ is temperature difference parameter.

In this study, quantities of interest include the skin friction coefficient C_{fx} , Nusselt number Nu_x , and local Sherwood number Sh_x , that clarified by [12, 38],

$$C_{fx} = \frac{v}{u_w^2(x)} \left(\frac{\partial u}{\partial y} \right) \Big|_{y=0}, \quad Nu_x = -\frac{x}{\Delta T} \left(\frac{\partial T}{\partial y} \right) \Big|_{y=0}, \quad Sh_x = -\frac{x}{\Delta C} \left(\frac{\partial C}{\partial y} \right) \Big|_{y=0}, \tag{12}$$

and by simplifying (12) with (6), we finally get,

$$Re_x^{1/2}C_{fx} = f''(0), \quad Re_x^{-1/2}Nu_x = -\theta'(0), \quad Re_x^{-1/2}Sh_x = -\varphi'(0).$$
 (13)

3 Results and Discussions

To justify the correctness of our mathematical model, we notice that the BVP in (7) can be reduced to,

$$f''' + ff'' - (f')^2 = 0,$$

$$f(0) = 0, f'(0) = \lambda, \quad f'(\eta) \to 1 \text{ as } \eta \to \infty,$$
(14)

where M=0 and $\Lambda=1$, so that we can compare the numerical result as in (14) with those reported by Mahapatra and Gupta [30] and Nazar et al. [33], as listed in Table 1. Further, we consider Ec=Nb=Nt=0 and the BVP in (8) can simplify to,

$$\theta'' + Prf\theta' = 0,$$

$$\theta(0) = 1, \quad \theta(\eta) \to 0 \text{ as } \eta \to \infty,$$
(15)

Table 1: Comparison of f''(0) for selected values of λ .

λ	f''(0)				
	Mahapatra and Gupta [30]	Nazar et al. [33]	Current outcomes		
0.1	-0.9694	-0.9694	-0.96937029		
0.2	-0.9181	-0.9181	-0.91811665		
1.5	-0.6673	-0.6673	-0.66734002		
2.0	2.0175	2.0176	2.01749549		
3.0	4.7293	4.7296	4.72952736		

that followed the analytical solution of,

$$\theta(\eta) = 1 - \frac{\int_0^{\eta} exp[-Pr f(s)]ds}{\int_0^{\infty} exp[-Pr f(\eta)]d\eta},\tag{16}$$

with

$$\theta'(0) = -\frac{1}{\int_0^\infty exp[-Prf(\eta)]d\eta}.$$
(17)

The reduced heat transfer $-\theta'(0)$ in (17) is compared with the analysis by Bachok et al. [6], as shown in Table 2. The agreement between these results confirms the validity of the current findings, which justify the present mathematical model is suitable for analysing fluid flow and heat transfer in this study.

Pr	M	$\theta'(0)$			
Γ/		Bachok et al. [6]	Current outcomes		
	1.0	-0.5061	-0.50609711		
1.0	2.0	-0.3826	-0.38257961		
	3.0	-0.3120	-0.31183328		
	1.0	-1.3389	-1.33896471		
7.0	2.0	-1.0124	-1.01234008		
	3.0	-0.8253	-0.82535314		

Table 2: Comparison of $\theta'(0)$ for selected values of Pr and M.

The BVPs in (7)–(9) with boundary conditions in (10) are numerically solved via MATLAB's bvp4c solver with an initial mesh of 150 points and a variable step size is employed to adjust dynamically based on error estimates. To ensure numerical accuracy, the convergence of the analysis is achieved when the residual error falls below 10^{-7} [4]. Further, Table 3 provides the range of the key parameters where the skin friction coefficient $Re_x^{1/2}C_{fx}$, Nusselt number $Re_x^{-1/2}Nu_x$, and concentration gradient which represent by local Sherwood number $Re_x^{-1/2}Sh_x$ for varies M are presented in Figure 3. As M increases, the field of magnetic interacts with the electrically conducting fluid, creating a Lorentz force, which causes a slowdown in fluid flow and hence reduces both $Re_x^{1/2}C_{fx}$ and $Re_x^{-1/2}Nu_x$. The observed behaviour implies that applying a magnetic field reduces the shear stress at the surface by damping the fluid motion, and also hinders heat transfer efficiency.

However, a stronger M seems to stabilize the flow, thereby steepening the $Re_x^{-1/2}Sh_x$ near the surface and increase the mass transfer rate. This behaviour is consistent with the suppression of turbulence or mixing by magnetic forces, which can confine the $Re_x^{-1/2}Sh_x$ closer to the boundary layer. The profiles of velocity $f'(\eta)$, temperature $\theta(\eta)$, and concentration $\varphi(\eta)$ for varies M are portrayed further in Figure 4. The field of magnetic yields a stronger braking force (Lorentz force) on the fluid as M increases, which slows down the velocity. With lower velocity, the flow cannot mix heat efficiently, so the temperature decreases because heat transfer relies more on slower conduction. At the same time, weaker flow also means less mixing of species, so the concentration increases because diffusion dominates and allows more buildup in certain areas.

Table 3: The key parameters and their respective range [38].

Parameter	Range
Magnetic parameter, M	$0.1 \le M \le 0.8$
Electric field parameter, Λ	$0.1 \le \Lambda \le 0.4$
Stretching parameter, λ	$0 \le \lambda \le 1.6$
Activation energy parameter, A_E	$0.2 \le A_E \le 0.8$
Brownian motion parameter, Nb	$0.1 \leq Nb \leq 0.5$
Thermophoresis parameter, Nt	$0.1 \le Nt \le 0.8$
Eckert number, Ec	$0.1 \le Ec \le 0.4$
Temperature difference parameter, τ	$0.1 \le \tau \le 0.8$

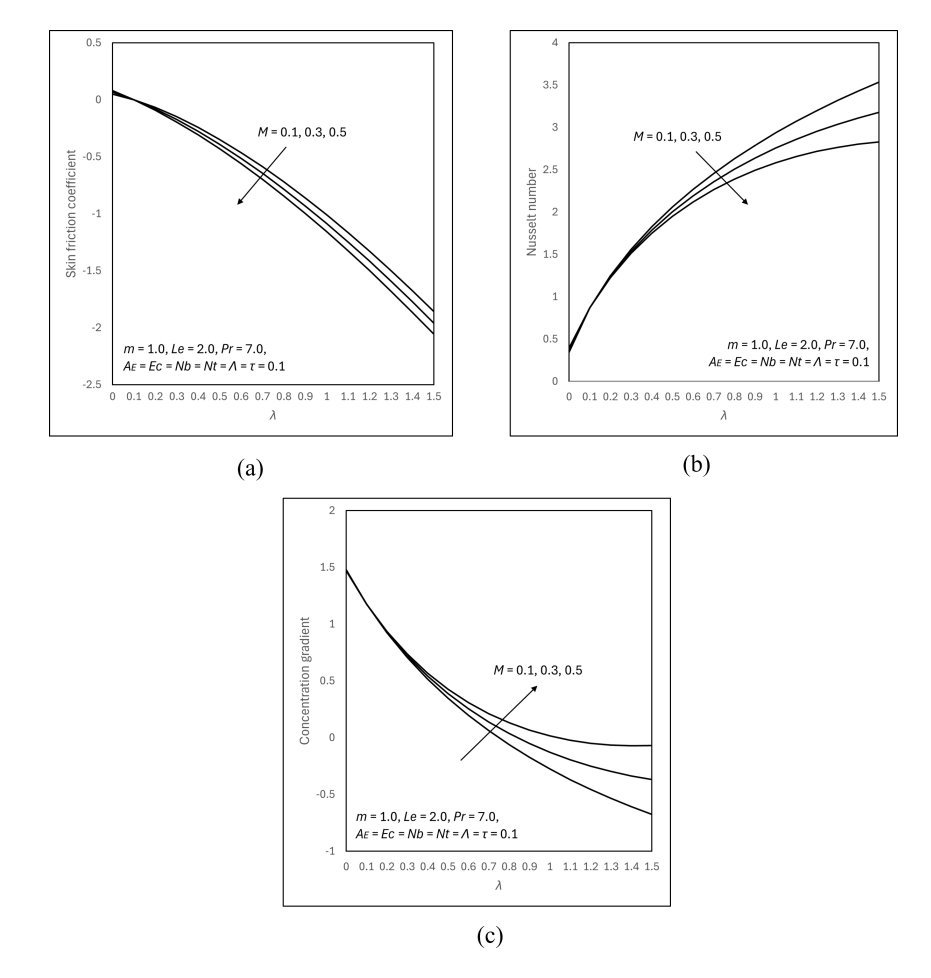


Figure 3: Varies M on: (a) $Re_x^{1/2}C_{fx}$, (b) $Re_x^{-1/2}Nu_x$, and (c) $Re_x^{-1/2}Sh_x$.

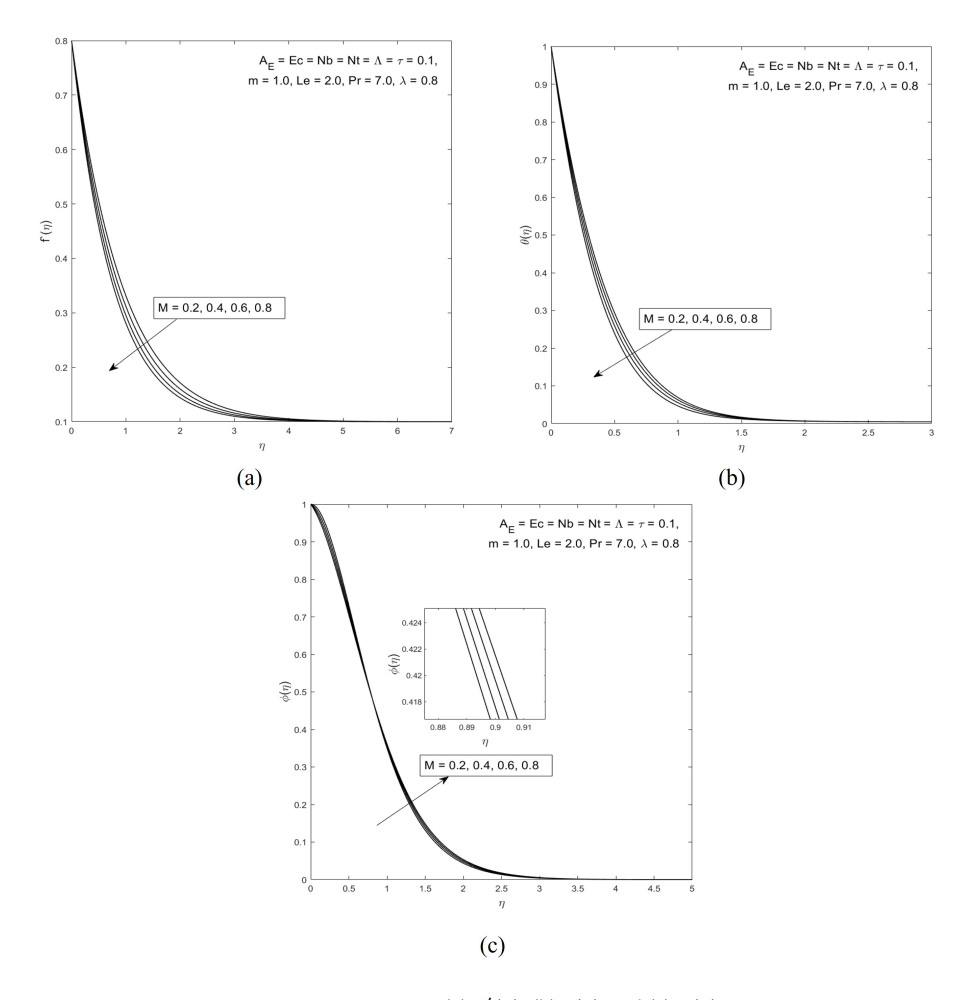


Figure 4: Varies M on: (a) $f'(\eta)$, (b) $\theta(\eta)$, and (c) $\varphi(\eta)$.

Figure 5 illustrates $Re_x^{1/2}C_{fx}$, $Re_x^{-1/2}Nu_x$, and $Re_x^{-1/2}Sh_x$ for varies electric field parameter, Λ . The presence of Λ alters the flow dynamics through additional body forces (such as Coulomb forces or Lorentz forces). For a fluid under an electric field, Λ changes changes the velocity gradient at the wall and directly influencing the $Re_x^{1/2}C_{fx}$. Λ also can influence the temperature distribution in the fluid by affecting the flow (velocity field), which in turn changes the convective heat transfer. Hence, increasing Λ can enhances both $Re_x^{1/2}C_{fx}$ and $Re_x^{-1/2}Nu_x$. Meanwhile, decreasing Λ will reduces $Re_x^{-1/2}Sh_x$. Λ reduces the flow velocity near the surface (e.g., through damping effects in electrically conductive fluids), the convective transport of mass decreases which in weaker mass transfer, reflected by a decrease in $Re_x^{-1/2}Sh_x$. Profiles for $f'(\eta)$, $\theta(\eta)$, and $\varphi(\eta)$ for varies Λ are then shown in Figure 6. As Λ increases, the velocity profile increases because the electromagnetic force drives the fluid motion. This stronger flow enhances convective heat transfer and, along with Joule heating, raises the temperature profile. At the same time, the increased velocity improves mixing, reducing concentration gradients and causing a decline in the concentration profile.

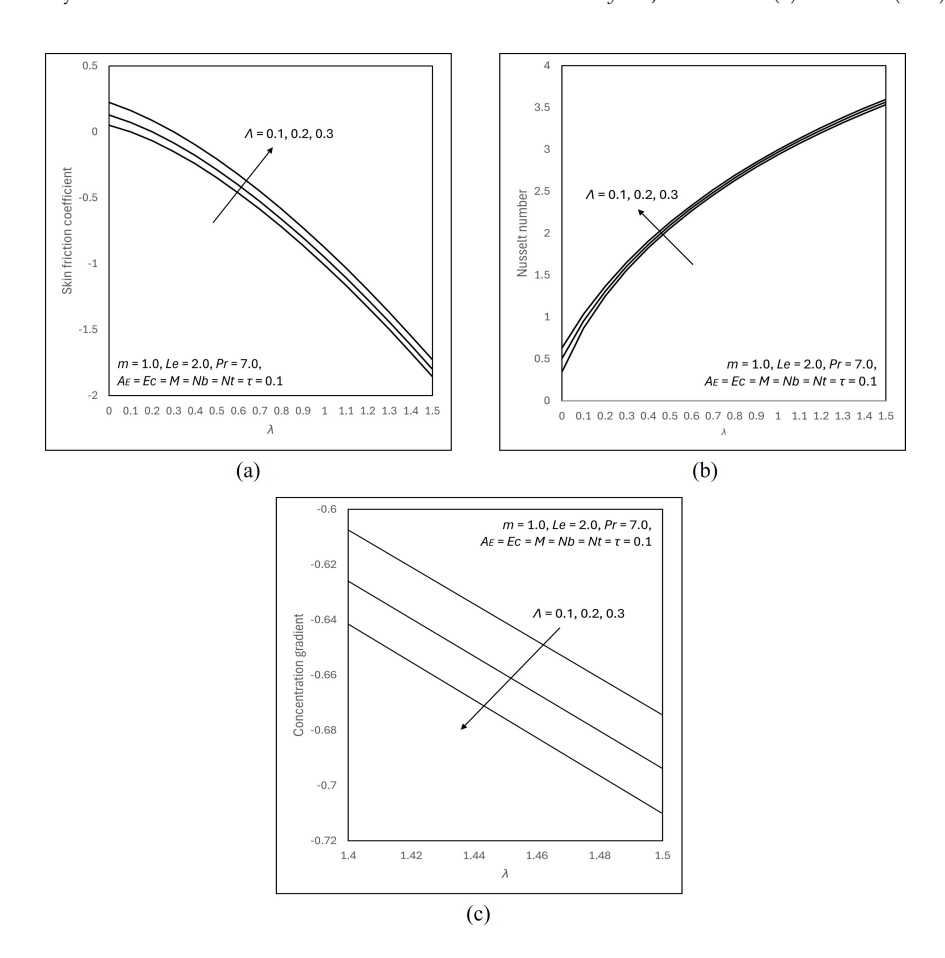
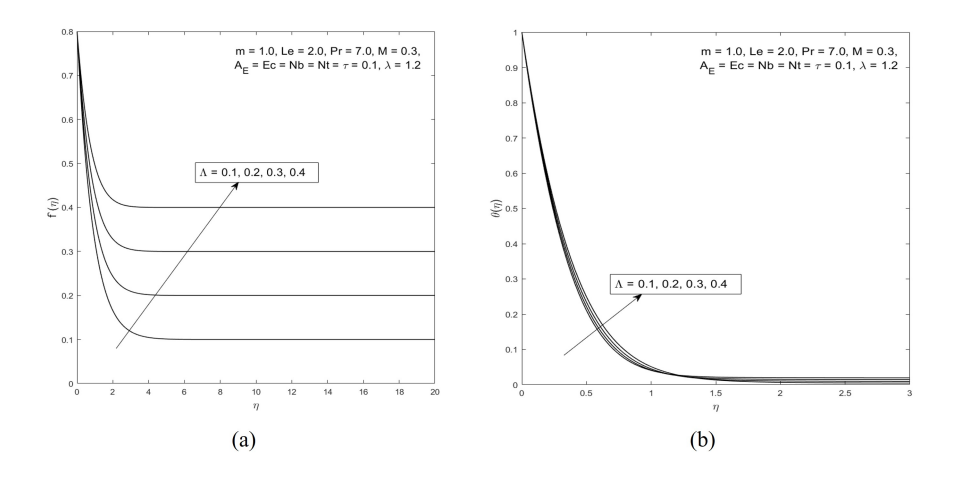


Figure 5: Varies Λ on: (a) $Re_x^{1/2}C_{fx}$, (b) $Re_x^{-1/2}Nu_x$, and (c) $Re_x^{-1/2}Sh_x$.



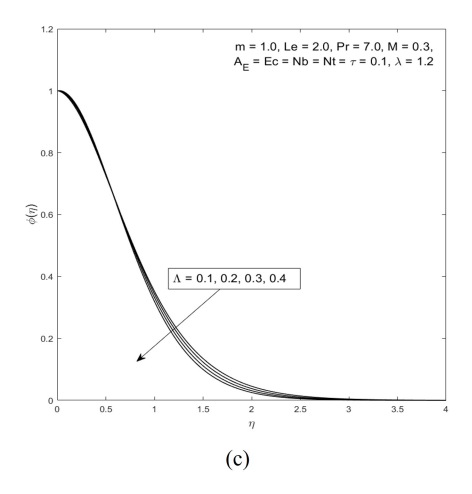


Figure 6: Varies Λ on: (a) $f'(\eta)$, (b) $\theta(\eta)$, and (c) $\varphi(\eta)$.

Figure 7 further plots the profiles for $f'(\eta)$, $\theta(\eta)$, and $\varphi(\eta)$ for varies λ . As λ increases, the fluid is stretched more, which causes both velocity and concentration to decrease. At the same time, the temperature increases due to enhanced heat transfer from the increased surface area created by the stretching, which improves convective heat exchange.

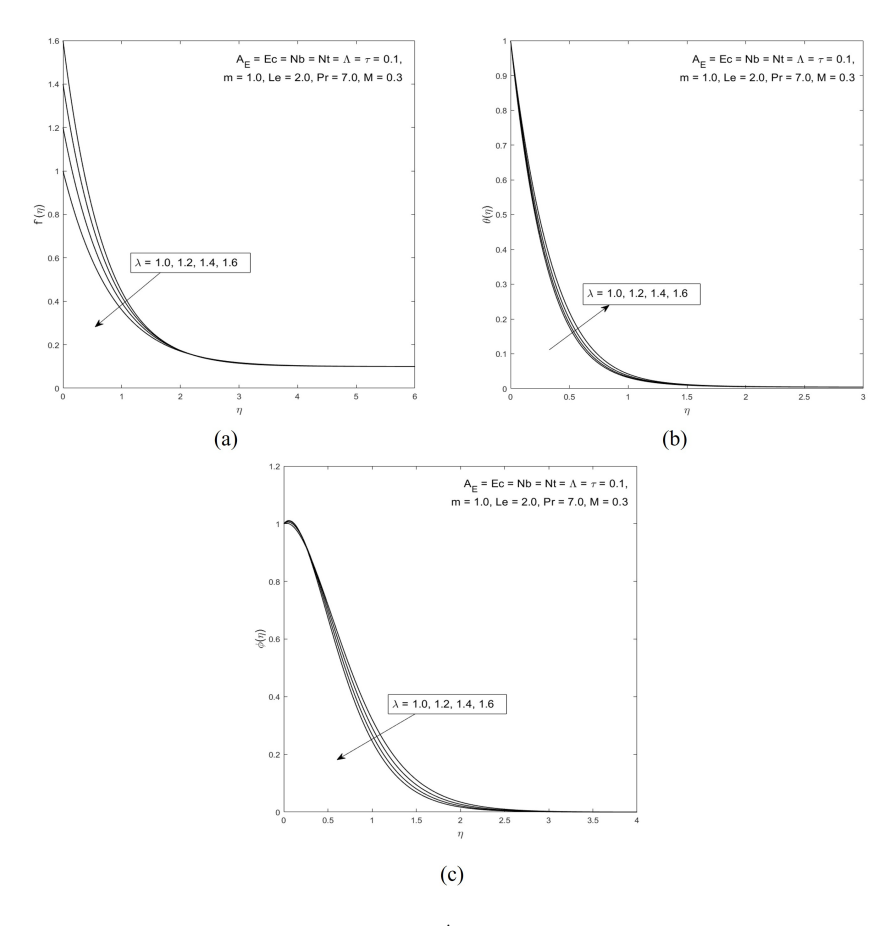


Figure 7: Varies λ on: (a) $f'(\eta)$, (b) $\theta(\eta)$, and (c) $\varphi(\eta)$.

The local Sherwood number $Re_x^{-1/2}Sh_x$ and concentration profiles $\varphi(\eta)$ against activation energy parameter A_E are presented in Figure 8. By definition, A_E refers to the energy needed to start a chemical reaction or process, like diffusion, reaction rates, or species transport. Increasing A_E reduces the rate at which species diffuse or react in the fluid, making it harder for species to move or undergo reactions. As a result, the $Re_x^{-1/2}Sh_x$ becomes steeper or more localized, meaning species are less uniformly distributed. However, the slower diffusion and reduced reaction rates prevent the species from dispersing, causing the $\varphi(\eta)$ profile to rise. Figure 9 then illustrates $\theta(\eta)$ and $\varphi(\eta)$ profiles for varies Ec. An increase in Ec affects fluid dynamics by altering temperature and concentration profiles. Higher Ec signifies stronger viscous dissipation, which can reduce temperature profiles when heat is rapidly dissipated or distributed through high thermal conductivity systems. Simultaneously, the increased energy enhances molecular diffusion, thickening the concentration boundary layer and raising $\varphi(\eta)$.

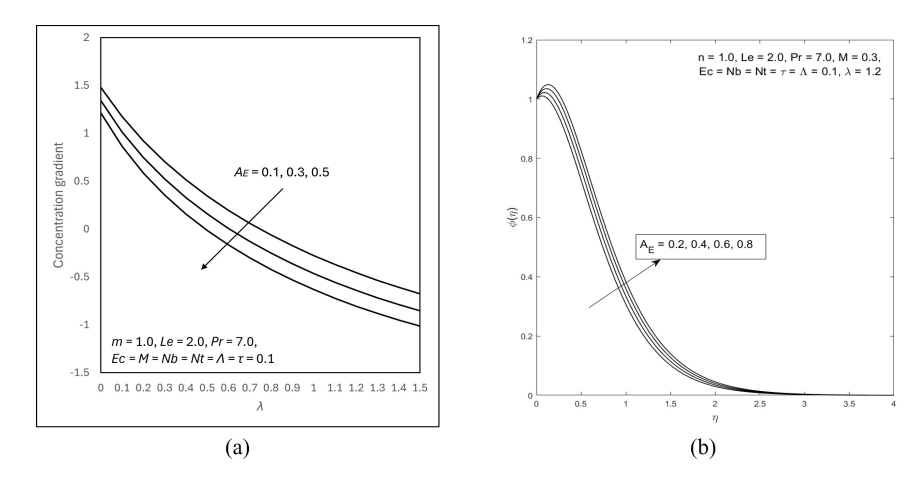


Figure 8: Varies A_E on: (a) $Re_x^{-1/2}Sh_x$, and (b) $\varphi(\eta)$.

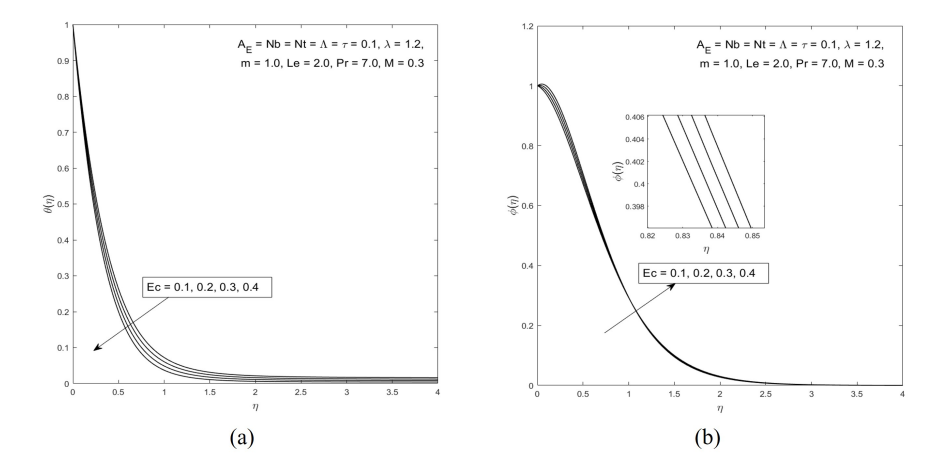


Figure 9: Varies Ec on: (a) $\theta(\eta)$, and (b) $\varphi(\eta)$.

The quantities of interest for $Re_x^{-1/2}Nu_x$ and $Re_x^{-1/2}Sh_x$, as well as the profiles of $\theta(\eta)$ and $\varphi(\eta)$ for varies Nb are shown in Figure 10. Nb refers to irregular particle movement dispersed in a fluid, caused by interactions with adjacent particles, which then transferring energy in the form

of heat. As Nb increases, random nanoparticle movement lowers thermal gradients near surfaces. This reduces the Nusselt number $Re_x^{-1/2}Nu_x$ and the temperature profile near the surface. At the same time, increased Nb steepens the nanoparticle concentration gradient, promoting $Re_x^{-1/2}Sh_x$ leading to a more pronounced concentration profile $\varphi(\eta)$. The plots of $Re_x^{-1/2}Nu_x$, $Re_x^{-1/2}Sh_x$, $\theta(\eta)$, and $\varphi(\eta)$ for varies Nt are further presented in Figure 11. Increment of Nt enhances the thermophoretic motion, causing nanoparticles to emigrate from hotter areas. This disrupts the thermal gradient near the surface, leading to a reduction in $Re_x^{-1/2}Nu_x$, as well as lowering the temperature profile $\theta(\eta)$ in the boundary layer. Increased Nt also result in a flattening the $Re_x^{-1/2}Sh_x$ and thinner concentration boundary layer as particles migrate more efficiently, decreasing the overall concentration profile $\varphi(\eta)$. Additionally, Figure 12 presents the local Sherwood number $Re_x^{-1/2}Sh_x$ and concentration profiles $\varphi(\eta)$ for varies τ . The temperature difference parameter τ amplifies thermal diffusion effects, which enhances the Soret effect (thermo-diffusion). This drives particles from hotter to cooler regions, steepening $Re_x^{-1/2}Sh_x$. This also elevates the concentration levels in certain regions of the boundary layer, then increases the thickness of the concentration profile.

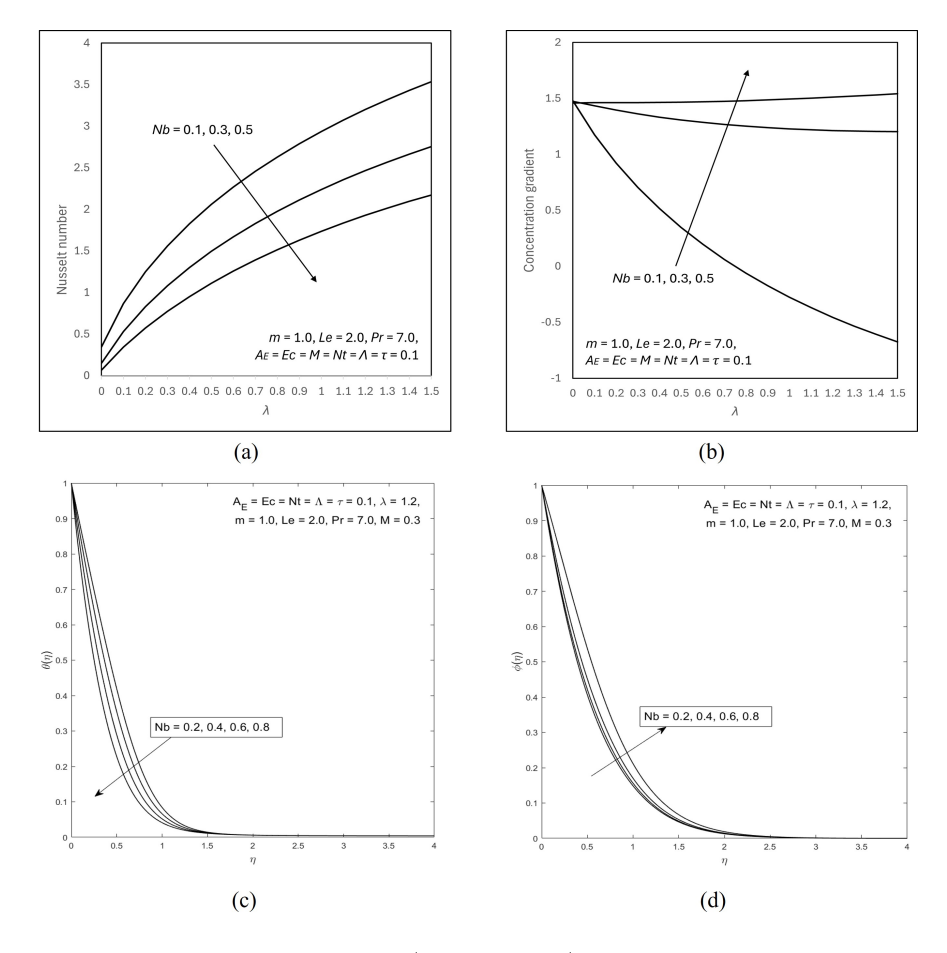


Figure 10: Varies Nb on: (a) $Re_x^{-1/2}Nu_x$, (b) $Re_x^{-1/2}Sh_x$, (c) $\theta(\eta)$, and (d) $\varphi(\eta)$.

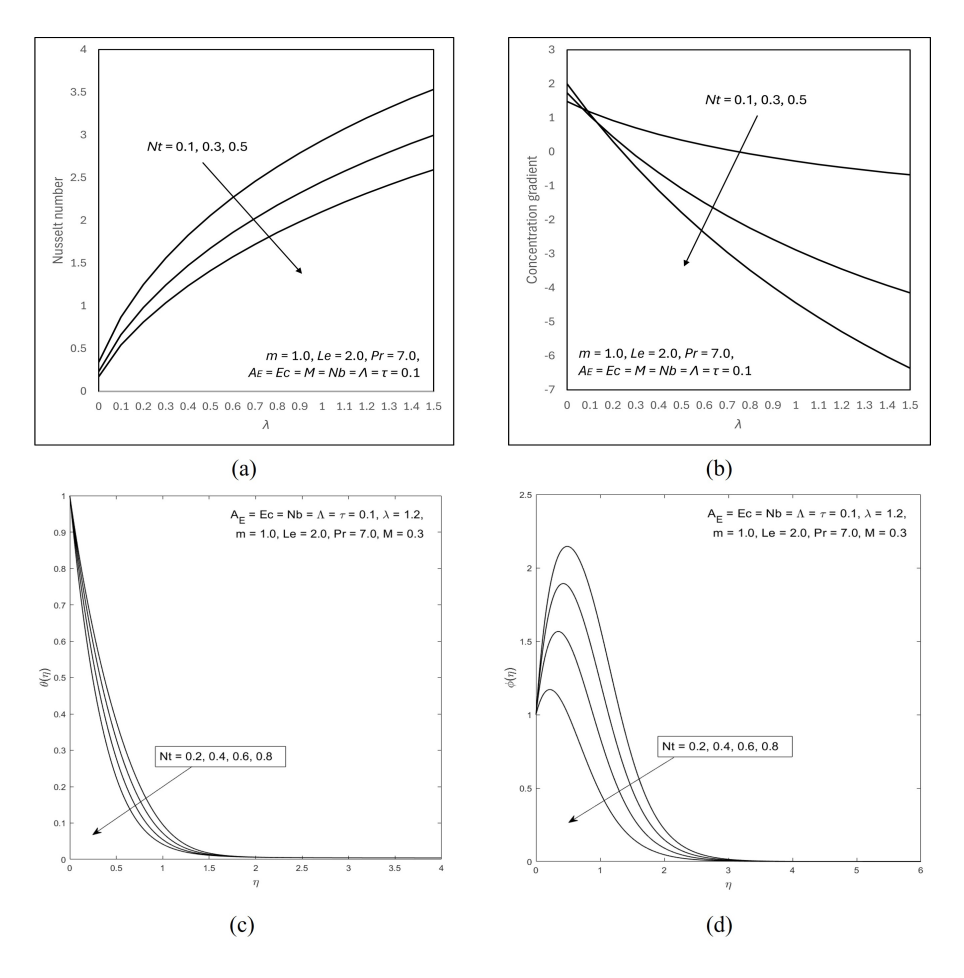


Figure 11: Varies Nt on: (a) $Re_x^{-1/2}Nu_x$, (b) $Re_x^{-1/2}Sh_x$, (c) $\theta(\eta)$, and (d) $\varphi(\eta)$.

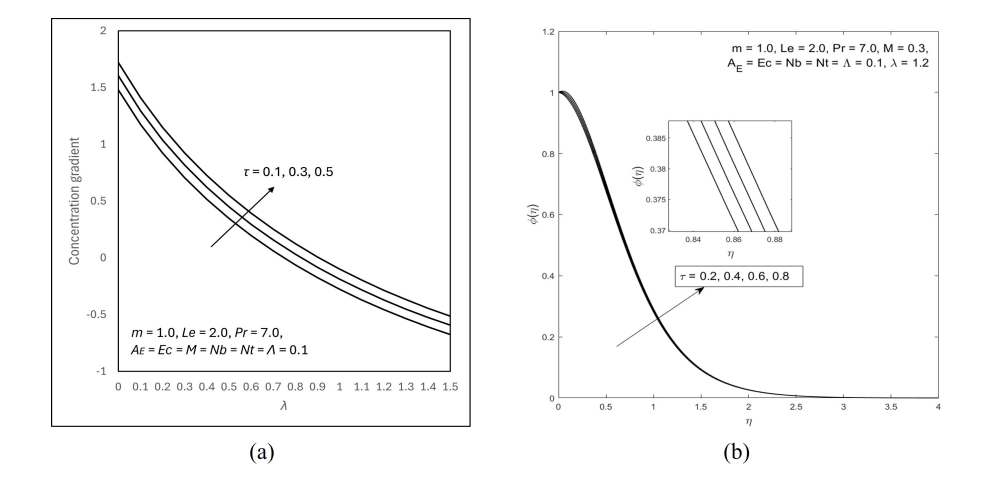


Figure 12: Varies τ on: (a) $Re_x^{-1/2}Sh_x$, and (b) $\varphi(\eta)$.

Further, Figures 13 and 14 present the streamline flows for electrical field parameter Λ , and magnetic parameter M, respectively. A streamline is a curve that represents the path of a fluid element follows in a flow field at any given point. It exhibits the direction of the fluid velocity at every point, meaning the tangent of the streamline aligns with the local velocity vector of the fluid. Here, the streamline flows can identify areas of high or low velocity, and we can further observe the influences of varies parameters on the flow. From Figure 13, when Λ increases, the streamlines move closer and come into contact which indicates a higher velocity gradient and localized flow compression. This suggests that the electric field strengthens the flow intensity and potentially reducing re-circulation zones. In the meantime, as M increases, the streamlines expand and causes the flow to spread out. This may be due to the magnetic force inducing a damping effect on the fluid and reduce velocity gradients at some point.

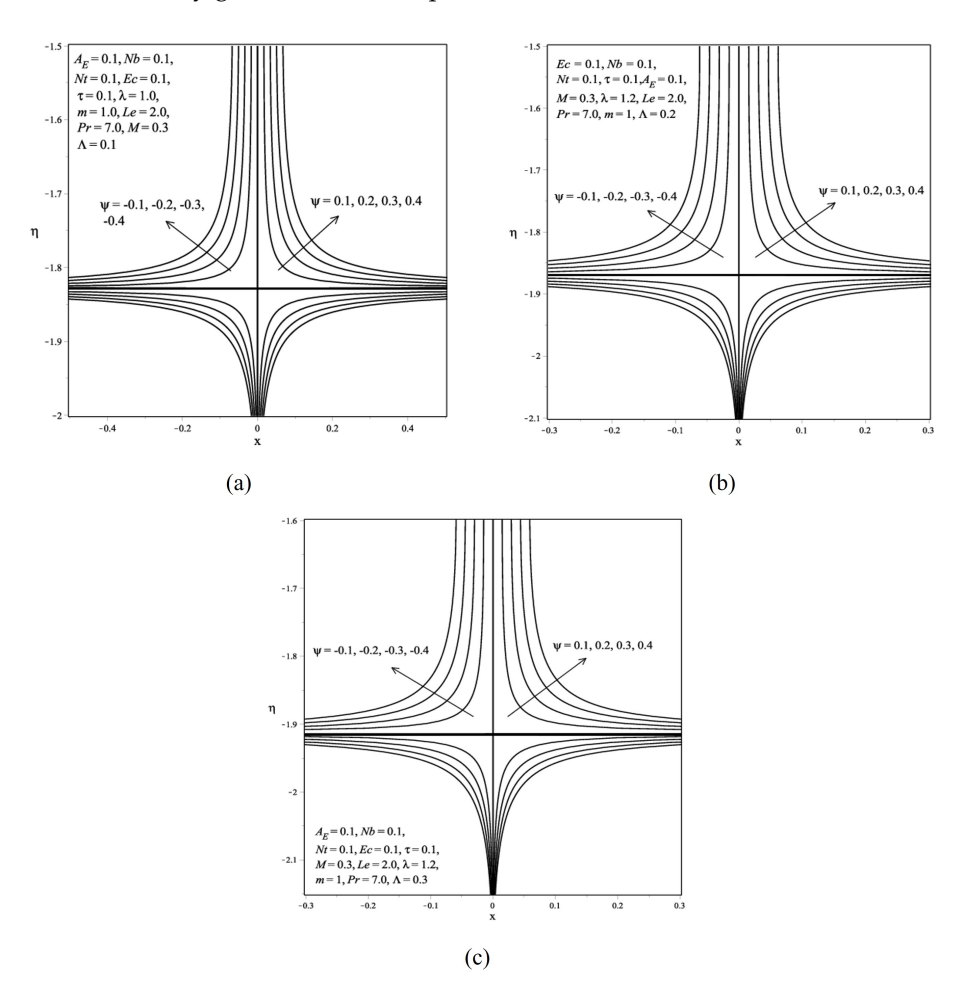


Figure 13: Streamline flows for: (a) $\Lambda=0.1$, (b) $\Lambda=0.2$, and (c) $\Lambda=0.3$.

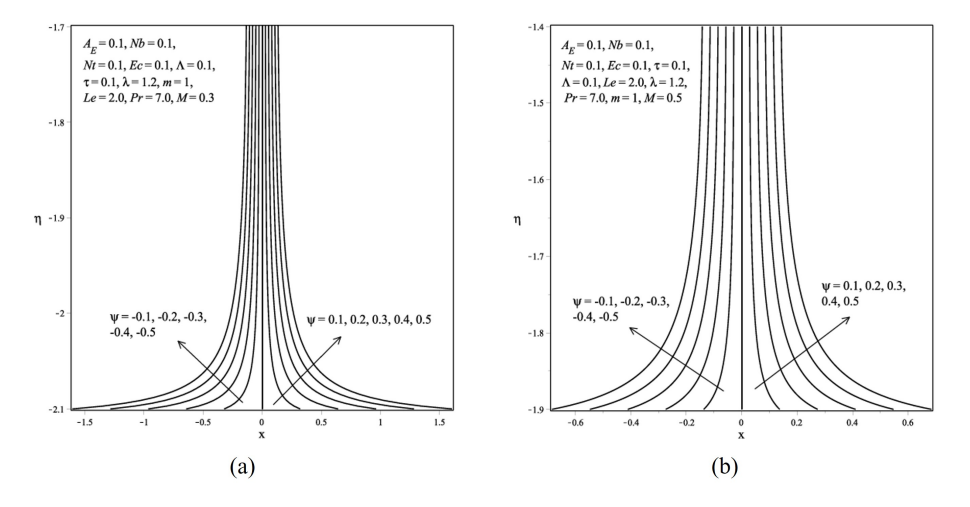


Figure 14: Streamline flows for: (a) M=0.3, and (b) M=0.5.

4 Response Surface Methodology (RSM)

Response Surface Methodology (RSM), also known as the Box-Wilson method [8], is a technique that combines statistical and mathematical tools based on experimental design. It is useful for identifying which independent variables have a significant impact on a response (dependent variable) in problems involving multiple independent variables. The relationship between the response and the independent variables is expressed as follows [29]:

$$res = F(X_1, X_2, X_3, \dots, X_t) \pm Er,$$
 (18)

where *res* is the response, F is the unknown function of response with $X_1, X_2, X_3, \ldots, X_t$ as independent variables, and Er is the statistical error. The general quadratic model can be expressed as follows:

$$res = a_0 + \sum_{i=1}^{t} a_i x_i + \sum_{i=1}^{t} a_{ii} x_i^2 + \sum_{i=1}^{t-1} \sum_{j=1}^{t} a_{ij} x_i x_j,$$
(19)

with a_0 , a_i , a_{ii} , and a_{ij} are the intercept, linear, quadratic and bilinear two-factor terms, respectively.

RSM can also be used to determine the best conditions for a response and to predict process outcomes [29, 20]. The optimization process through RSM involves several steps: defining the independent variables and their range, selecting the experimental design, predicting and validating the model equation, and finally determining the optimal point. In this study, RSM is applied to evaluate the effects of M, Λ , and λ in optimizing heat transfer rate $Re_x^{-1/2}Nu_x$. The coded symbols A, B, and C represent M, Λ , and λ with values set at low (-1), middle (0), and high (1), as shown in Table 4. Other parameters are kept constant at Le=2.0, $A_E=Ec=Nb=Nt=\tau=0.1$, and Pr=7.0.

Table 4: Independent parameters and their range.

Level	Parameter				
Level	M[A]	Λ [B]	λ [C]		
-1 (Low)	0.1	0.1	1.0		
0 (Medium)	0.3	0.2	1.2		
1 (High)	0.5	0.3	1.4		

Computational models are employed to generate the output responses by systematically varying the values of factor. Additionally, a face-centred composite design is utilized to structure the experimental setup, with the trials number N calculated via formula $N=2^F+2F+C$, where F=3 (factors number) and C=6 (centre points). For the three specified parameters, Table 5 lists a total of 20 runs [29]. The numerical results presented in Table 6 are then examined through analysis of variance (ANOVA) in Minitab.

Table 5: Experimental design for $Re_x^{-1/2}Nu_x$.

Runs	Uncoded parameter			Response $Re_x^{-1/2}Nu_x$	
Kulis	M	Λ	λ	Response $ne_x - Nu_x$	
1	0.1	0.2	1.2	3.230587362	
2	0.1	0.3	1.0	2.995491119	
3	0.1	0.1	1.4	3.429776458	
4	0.3	0.2	1.4	3.197365670	
5	0.3	0.2	1.2	3.033187458	
6	0.5	0.3	1.4	3.063720920	
7	0.5	0.1	1.4	2.801904454	
8	0.3	0.2	1.0	2.827771204	
9	0.5	0.3	1.0	2.792847855	
10	0.3	0.3	1.2	3.104330696	
11	0.3	0.2	1.2	3.033187458	
12	0.5	0.2	1.2	2.842059214	
13	0.1	0.1	1.0	2.935605467	
14	0.3	0.2	1.2	3.033187458	
15	0.1	0.3	1.4	3.492691126	
16	0.3	0.1	1.2	2.954112673	
17	0.3	0.2	1.2	3.033187458	
18	0.3	0.2	1.2	3.033187458	
19	0.3	0.2	1.2	3.033187458	
20	0.5	0.1	1.0	2.582332717	

Table 6: ANOVA for the full model of $Re_x^{-1/2}Nu_x$.

Source	DF	Adj SS	Adj MS	F-value	P-value
Model	9	0.848119	0.094235	2490.50	0.000
Linear	3	0.798841	0.266280	7037.37	0.000
A	1	0.400515	0.400515	10584.97	0.000
B	1	0.055555	0.055555	1468.22	0.000
C	1	0.342772	0.342772	9058.92	0.000
Square	3	0.002272	0.000757	20.01	0.000
A*A	1	0.000027	0.000027	0.72	0.415
B*B	1	0.000043	0.000043	1.13	0.313
C*C	1	0.001167	0.001167	30.84	0.000
2-Way	3	0.047006	0.015669	414.10	0.000
Interaction					
A*B	1	0.015272	0.015272	403.60	0.000
A*C	1	0.031366	0.031366	828.95	0.000
B*C	1	0.000369	0.000369	9.75	0.011
Error	10	0.000378	0.000038		
Lack-of-Fit	5	0.000378	0.000076	*	*
Pure Error	5	0.000000	0.00000		
Total	19	0.848498			

Further, the model considered well-fitting as their residuals follow a normal distribution. The model achieves statistical significance if the sources' P-value is under 0.05 according to Myres et al. [32]. The several factors shown in Table 6 are excluded since P-values is exceed 0.05 when developing the reduced model (Table 7).

Source	DF	Adj SS	Adj MS	F-value	P-value
Model	7	0.848068	0.121153	3379.59	0.000
Linear	3	0.798841	0.266280	7427.99	0.000
A	1	0.400515	0.400515	11172.50	0.000
B	1	0.055555	0.055555	1549.72	0.000
C	1	0.342772	0.342772	9561.75	0.000
Square	1	0.002220	0.002220	61.92	0.000
C*C	1	0.002220	0.002220	61.92	0.000
2-Way	3	0.047006	0.015669	437.09	0.000
Interaction					
A*B	1	0.015272	0.015272	426.00	0.000
A*C	1	0.031366	0.031366	874.96	0.000
B*C	1	0.000369	0.000369	10.29	0.008
Error	12	0.000430	0.000036		
Lack-of-Fit	7	0.000430	0.000036	*	*
Pure Error	5	0.000000	0.000000		
Total	19	0.848498			

Table 7: ANOVA for the reduced model of $Re_x^{-1/2}Nu_x$.

Consequently, the reduced models are statistically well-fitted to provide the optimum solutions for $Re_x^{-1/2}Nu_x$. As a result, (19) then can be derived to finally obtain the following quadratic regression equations for $Re_x^{-1/2}Nu_x$,

$$Nu_x = 0.964 + 0.4409M - 0.317\Lambda + 2.592\lambda - 0.5268\lambda^2 + 2.185M\Lambda - 1.5654M\lambda + 0.340\Lambda\lambda.$$
(20)

Further analysis of the interactive impacts of these parameters is conducted via contour and surface plots (see Figures 15 and 16). From Figure 15, the elevation in A(M) reduces the response. Conversely, the amplification of response occurs at higher values of $B(\Lambda)$ and $C(\lambda)$. Thus, $Re_x^{-1/2}Nu_x$ is improved by the increase in electric field Λ and stretching λ parameters.

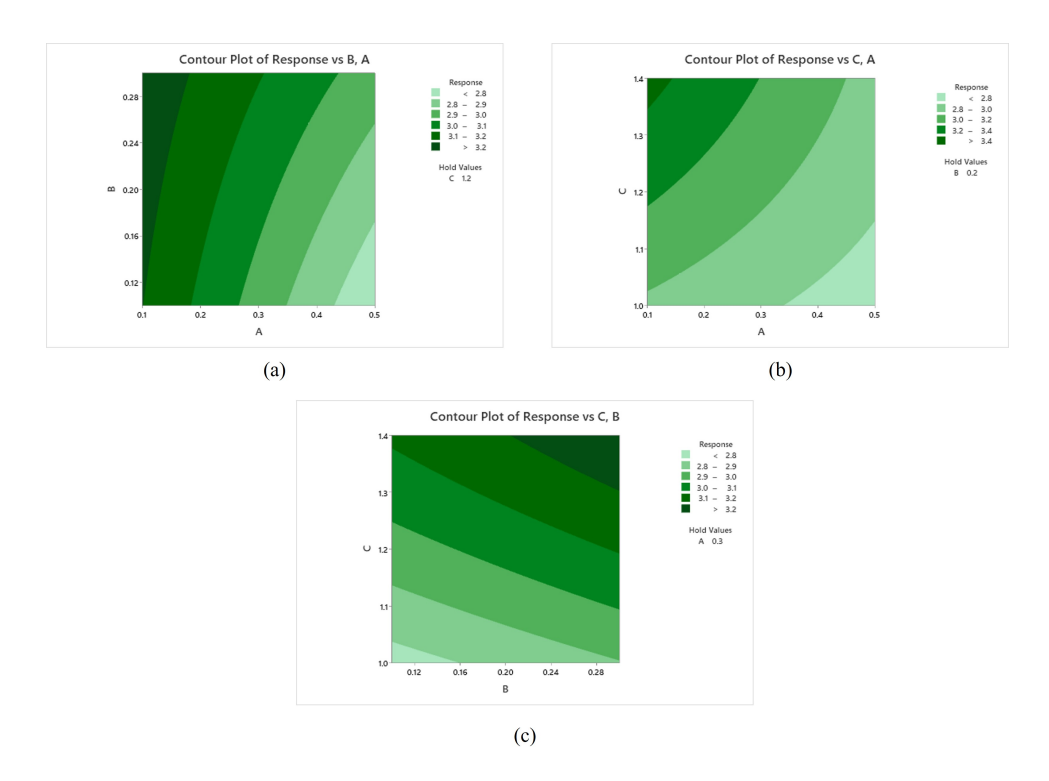


Figure 15: Contour plots for interaction between: (a) *A* and *B*, (b) *A* and *C*, and (c) *B* and *C*.

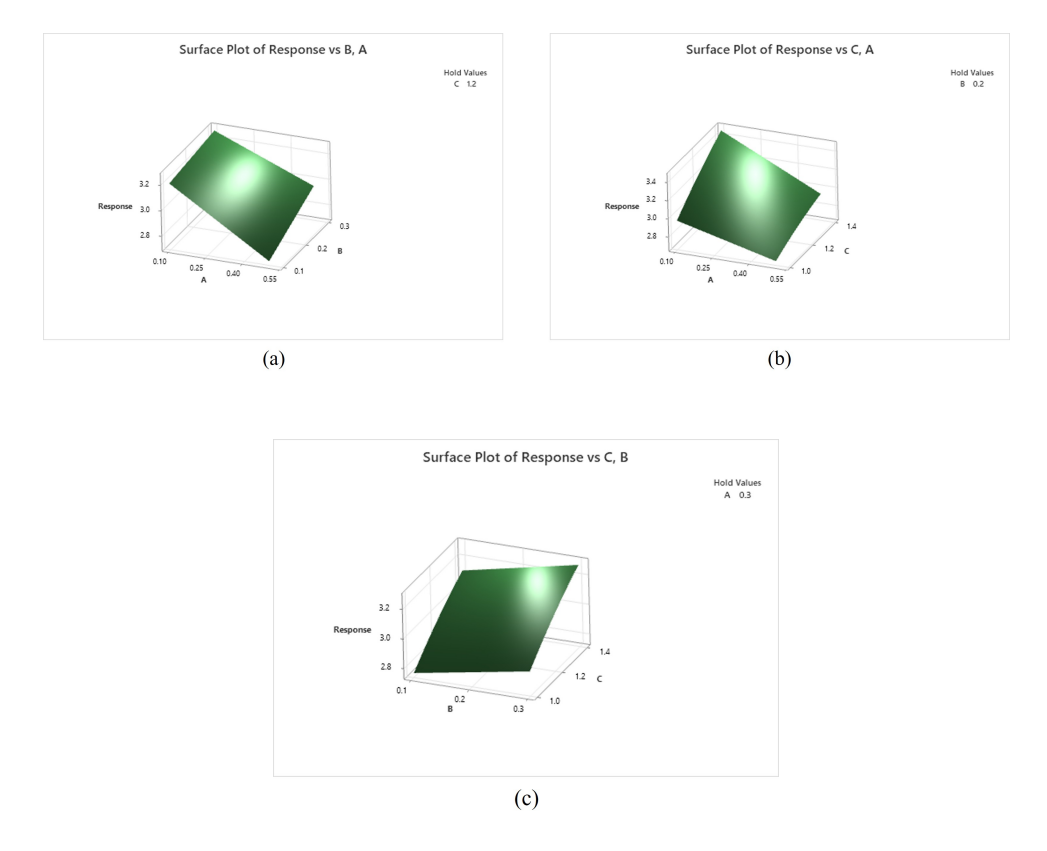


Figure 16: Surface plots for interaction between: (a) *A* and *B*, (b) *A* and *C*, and (c) *B* and *C*.

Additionally, the impact of these parameters on optimizing the heat transfer rate is analyzed via optimization, with the results shown in Table 8. The heat transfer rate is considered optimized when the maximum value of $Re_x^{-1/2}Nu_x$ is attained, when M=0.1, $\Lambda=0.3$, and $\lambda=1.4$.

Table 8: The optimal solution of $Re_x^{-1/2}Nu_x$.

Solution	\boldsymbol{A}	В	С	Response fit	Composite desirability
1	0.1	0.3	1.4	3.49747	1

5 Conclusions

This study examines electrically conductive magnetohydrodynamic (MHD) flow over a shrinking sheet with Arrhenius activation energy using a modified Buongiorno approach. Key variables such as M, Λ , A_E , λ , Ec, Nb, Nt, and τ in non-dimensional form are included in the model. Numerical analysis is performed using bvp4c function in MATLAB, while Response Surface Methodology (RSM) in Minitab is applied for optimization process. The findings reveal the influence of key parameters on flow, heat, and mass transfer characteristics, where the main conclusions are listed below:

- Increasing the magnetic parameter M lowers the skin friction coefficient $Re_x^{1/2}C_{fx}$.
- A higher electric field parameter Λ increases $Re_x^{1/2}C_{fx}$ and $Re_x^{-1/2}Nu_x$ while reducing $Re_x^{-1/2}Sh_x$. The activation energy parameter A_E also diminishes $Re_x^{-1/2}Sh_x$.
- The stretching parameter λ raises temperature profiles but reduces concentration profiles. The parameter τ has opposite effect on concentration profiles.
- Increasing Brownian motion Nb, thermophoresis Nt, and Eckert number Ec reduces profiles while increases concentration profiles.
- For the RSM analysis, the maximum heat transfer rate is achieved when Λ and λ are in high position, while M is in low value.

It is worth noting that this research is relevant for cooling systems in high-temperature environments, such as in fusion reactors where the interaction of an electric field, magnetic field, and nanofluid properties can be adjusted to improve heat dissipation. The findings may also help in optimizing heat transfer in industrial plasma processing and electromagnetic casting. However, a limitation of this study is that it assumes a steady-state flow and does not account for time-dependent effects, which may be important in practical applications. To address this, future work will include unsteady flow analysis and experimental validation by using thermal imaging or temperature sensors to compare with real-world data. Additionally, different nanofluid base fluids and nanoparticles can be tested to examine their impact on heat and mass transfer performance.

Nomenclature

x, y Cartesian coordinates

 B_0 Magnitude of magnetic field (N/Am)

- $B_0(x)$ Electric field (Vc/m)
- D_B Brownian motion coefficient (m²/s)
- D_T Thermophoresis coefficient (m²/s)
- u, v Velocity components
- $u_e(x)$ Far field velocity
- $u_w(x)$ Stretching sheet velocity
- λ Stretching parameter
- (T,C) Temperature (K) and concentration $(mol/m^3/)$ of nanofluid
- (T_w, C_w) Temperature (K) and concentration (mol/m³/) of sheet surface
- (T_{∞}, C_{∞}) Temperature (K) and concentration (mol/m³/) of far-field
- k_r^2 Reaction rate
- k_1 Boltzmann constant (k)
- M Magnetic parameter
- Λ Electric field parameter
- Nb Brownian motion parameter
- Nt Thermophoresis parameter
- Pr Prandtl number
- Ec Eckert number
- Le Dimensionless Lewis number
- A_E Activation energy parameter
- au Temperature difference parameter

Subscripts:

- α Thermal diffusivity
- ρ Density (kgm⁻³)
- ν Kinematic viscosity (m²/s)
- μ Fluid viscosity (kg/ms)
- σ Electrical conductivity (S/m)
- ρC_p Heat capacity (J/g)

Acknowledgement The acknowledgement of this study is extended to Universiti Teknologi Malaysia (UTM) and Universiti Putra Malaysia (UPM) for their facilities and invaluable resources that contributed to the success of this research. This research was supported by the Potential Academic Staff (PAS) Grant under Universiti Teknologi Malaysia (UTM), with Grant number Q.K130000.2743.03K89.

Conflicts of Interest The authors confirm that they have reviewed and approved the final version of this manuscript. They further declare that there are no conflicts of interest or personal associations that could have influenced the objectivity of this research.

References

- [1] M. N. Abrar & S. Kosar (2024). Entropy generation and heat transfer characteristics in MHD Casson fluid flow over a wedge with viscous dissipation and thermal radiation. *ZAMM-Journal of Applied Mathematics and Mechanics/Zeitschrift für Angewandte Mathematik und Mechanik*, 104(8), Article ID: e202300666. https://doi.org/10.1002/zamm.202300666.
- [2] K. Ahmad & A. Ishak (2016). MHD flow and heat transfer of a Jeffrey fluid over a stretching sheet with viscous dissipation. *Malaysian Journal of Mathematical Sciences*, 10(S), 311–323.
- [3] A. Akbar, H. Ullah, K. S. Nisar, M. A. Z. Raja, M. Shoaib & S. Islam (2023). Intelligent computing paradigm for the Buongiorno model of nanofluid flow with partial slip and MHD effects over a rotating disk. *ZAMM-Journal of Applied Mathematics and Mechanics/Zeitschrift für Angewandte Mathematik und Mechanik*, 103(1), Article ID: e202200141. https://doi.org/10.1002/zamm.202200141.
- [4] B. Ali, R. A. Naqvi, A. Mariam, L. Ali & O. M. Aldossary (2020). Finite element study for magnetohydrodynamic (MHD) tangent hyperbolic nanofluid flow over a faster/slower stretching wedge with activation energy. *Mathematics*, 9(1), Article ID: 25. https://doi.org/10.3390/math9010025.
- [5] M. S. Anwar (2020). Numerical study of transport phenomena in a nanofluid using fractional relaxation times in Buongiorno model. *Physica Scripta*, 95(3), Article ID: 035211. https://doi.org/10.1088/1402-4896/ab4ba9.
- [6] N. Bachok, A. Ishak & I. Pop (2010). Melting heat transfer in boundary layer stagnation-point flow towards a stretching/shrinking sheet. *Physics letters A*, 374(40), 4075–4079. https://doi.org/10.1016/j.physleta.2010.08.032.
- [7] M. M. Bhatti & E. E. Michaelides (2021). Study of Arrhenius activation energy on the thermobioconvection nanofluid flow over a Riga plate. *Journal of Thermal Analysis and Calorimetry*, 143, 2029–2038. https://doi.org/10.1007/s10973-020-09492-3.
- [8] G. E. Box & K. B. Wilson (1992). On the experimental attainment of optimum conditions. In *Breakthroughs In Statistics: Methodology and Distribution*, pp. 270–310. Springer, New York.
- [9] J. Buongiorno (2006). Convective transport in nanofluids. *Transactions of The ASME*, 128, 240–250. https://doi.org/10.1115/1.2150834.
- [10] A. J. Chamkha & I. Pop (2004). Effect of thermophoresis particle deposition in free convection boundary layer from a vertical flat plate embedded in a porous medium. *International Communications In Heat and Mass Transfer*, 31(3), 421–430. https://doi.org/10.1016/j.icheatmasstransfer.2004.02.012.

- [11] Y. M. Chu, K. Al-Khaled, N. Khan, M. I. Khan, S. U. Khan, M. S. Hashmi, M. A. Iqbal & I. Tlili (2021). Study of Buongiorno's nanofluid model for flow due to stretching disks in presence of gyrotactic microorganisms. *Ain Shams Engineering Journal*, 12(4), 3975–3985. https://doi.org/10.1016/j.asej.2021.01.033.
- [12] Y. S. Daniel, Z. A. Aziz, Z. Ismail & F. Salah (2017). Entropy analysis in electrical magnetohydrodynamic (MHD) flow of nanofluid with effects of thermal radiation, viscous dissipation, and chemical reaction. *Theoretical and Applied Mechanics Letters*, 7(4), 235–242. https://doi.org/10.1016/j.taml.2017.06.003.
- [13] D. N. Dash, K. S. Arjun, D. N. Thatoi, R. Ali, M. K. Nayak & A. J. Chamkha (2024). Flow and heat transfer of nanofluids in a cylindrical permeable wavy channel embedded in porous medium using Buongiorno's model. *Modern Physics Letters B*, 38(20), Article ID: 2450157. https://doi.org/10.1142/S0217984924501574.
- [14] P. A. Davidson (2017). *Introduction To Magnetohydrodynamics*. Cambridge University Press, Cambridge, United Kingdom. https://doi.org/10.1017/CBO9780511626333.
- [15] R. Gandhi, B. Sharma & U. Khanduri (2023). Electromagnetohydrodynamics Casson pulsatile nanofluid flow through a bifurcated stenosed artery: Magnetically targeted drug delivery. *Journal of Applied Physics*, 134(18), Article ID: 184701. https://doi.org/10.1063/5.0172553.
- [16] K. Gangadhar, M. A. Kumari & A. J. Chamkha (2022). EMHD flow of radiative second-grade nanofluid over a Riga plate due to convective heating: Revised Buongiorno's nanofluid model. *Arabian Journal for Science and Engineering*, 47(7), 8093–8103. https://doi.org/10.1007/s13369-021-06092-7.
- [17] B. J. Gireesha, K. Gangadhar, M. S. P & S. Sindhu (2021). Entropy generation analysis of electrical magnetohydrodynamic flow of TiO₂-Cu/H₂O hybrid nanofluid with partial slip. *International Journal of Numerical Methods for Heat & Fluid Flow*, 31(6), 1905–1929. https://doi.org/10.1108/HFF-07-2020-0477.
- [18] T. S. Gregory, R. Cheng, G. Tang, L. Mao & Z. T. H. Tse (2016). The magnetohydrodynamic effect and its associated material designs for biomedical applications: A state-of-the-art review. *Advanced Functional Materials*, 26(22), 3942–3952. https://doi.org/10.1002/adfm.201504198.
- [19] V. R. R. Gurrampati & K. Vijaya (2022). The Buongiorno model with Brownian and thermophoretic diffusion for MHD Casson nanofluid over an inclined porous surface. *Journal of Naval Architecture and Marine Engineering*, 19(1), 31–45.
- [20] S. Hussain, K. Rasheed, A. Ali, N. Vrinceanu, A. Alshehri & Z. Shah (2022). A sensitivity analysis of MHD nanofluid flow across an exponentially stretched surface with non-uniform heat flux by response surface methodology. *Scientific Reports*, 12(1), Article ID: 18523. https://doi.org/10.1038/s41598-022-22970-y.
- [21] S. Jagadha, D. Gopal & N. Kishan (2020). Soret and Dufour effects of electrical MHD nanofluid with higher order chemical reaction. *Test Engineering and Management*, 82, 2250–2259.
- [22] M. C. Jayaprakash, M. D. Alsulami, B. Shanker & R. S. Varun Kumar (2025). Investigation of Arrhenius activation energy and convective heat transfer efficiency in radiative hybrid nanofluid flow. *Waves in Random and Complex Media*, 35(1), 273–285. https://doi.org/10.1080/17455030.2021.2022811.
- [23] F. Jensen (1985). Activation energies and the Arrhenius equation. *Quality and Reliability Engineering International*, 1(1), 13–17. https://doi.org/10.1002/qre.4680010104.

- [24] N. S. Khan, P. Kumam & P. Thounthong (2020). Second law analysis with effects of Arrhenius activation energy and binary chemical reaction on nanofluid flow. *Scientific Reports*, 10(1), Article ID: 1226. https://doi.org/10.1038/s41598-020-57802-4.
- [25] M. V. Krishna, N. A. Ahamad & A. J. Chamkha (2021). Hall and ion slip impacts on unsteady MHD convective rotating flow of heat generating/absorbing second grade fluid. *Alexandria Engineering Journal*, 60(1), 845–858. https://doi.org/10.1016/j.aej.2020.10.013.
- [26] M. V. Krishna, K. Bharathi & A. J. Chamkha (2018). Hall effects on MHD peristaltic flow of Jeffrey fluid through porous medium in a vertical stratum. *Interfacial Phenomena and Heat Transfer*, 6(3), 253–268. https://doi.org/10.1615/InterfacPhenomHeatTransfer.2019030215.
- [27] M. A. Kumar, S. Sreenadh, R. Saravana, R. H. Reddy & A. Kavitha (2016). Influence of velocity slip conditions on MHD peristaltic flow of a Prandtl fluid in a non-uniform channel. *Malaysian Journal of Mathematical Sciences*, 10(1), 35–47.
- [28] S. Lamidi, N. Olaleye, Y. Bankole, A. Obalola, E. Aribike & I. Adigun (2022). Applications of response surface methodology (RSM) in product design, development, and process optimization. In *Response Surface Methodology*, chapter 3. IntechOpen, Rijeka. https://doi.org/10.5772/intechopen.106763.
- [29] B. Mahanthesh, K. Thriveni, P. Rana & T. Muhammad (2021). Radiative heat transfer of nanomaterial on a convectively heated circular tube with activation energy and nanoparticle aggregation kinematic effects. *International Communications In Heat and Mass Transfer*, 127, Article ID: 105568. https://doi.org/10.1016/j.icheatmasstransfer.2021.105568.
- [30] T. R. Mahapatra & A. Gupta (2002). Heat transfer in stagnation-point flow towards a stretching sheet. *Heat and Mass Transfer*, 38(6), 517–521. https://doi.org/10.1007/s002310100215.
- [31] S. Mishra, K. Swain & R. Dalai (2024). Joule heating and viscous dissipation effects on heat transfer of hybrid nanofluids with thermal slip. *Iranian Journal of Science and Technology, Transactions of Mechanical Engineering*, 48(2), 531–539. https://doi.org/10.1007/s40997-023-00681-7.
- [32] R. H. Myers, D. C. Montgomery & C. M. Anderson-Cook (2016). *Response Surface Methodology: Process and Product Optimization Using Designed Experiments*. John Wiley & Sons, New Jersey.
- [33] R. Nazar, N. Amin, D. Filip & I. Pop (2004). Unsteady boundary layer flow in the region of the stagnation point on a stretching sheet. *International Journal of Engineering Science*, 42(11-12), 1241–1253. https://doi.org/10.1016/j.ijengsci.2003.12.002.
- [34] Nidhi & L. Kumar (2024). Magnetic dipole and mixed convective effect on boundary layer flow of ferromagnetic micropolar hybrid nanofluid. *Journal of Nanofluids*, 13(2), 435–445. https://doi.org/10.1166/jon.2024.2123.
- [35] N. H. A. Norzawary & N. Bachok (2024). MHD flow of hybrid carbon nanotubes over a stretching/shrinking sheet with slip: Heat transfer optimization. *Magnetohydrodynamics*, 60(3/4), 235–252. http://doi.org/10.22364/mhd.
- [36] W. Owhaib, M. Basavarajappa & W. Al-Kouz (2021). Radiation effects on 3D rotating flow of Cu-water nanoliquid with viscous heating and prescribed heat flux using modified Buongiorno model. *Scientific Reports*, 11(1), Article ID: 20669. https://doi.org/10.1038/s41598-021-00107-x.

- [37] M. Peleg, M. D. Normand & M. G. Corradini (2012). The Arrhenius equation revisited. *Critical Reviews In Food Science and Nutrition*, 52(9), 830–851. https://doi.org/10.1080/10408398. 2012.667460.
- [38] D. Qaiser & N. M. Khan (2024). Optimizing entropy in mixed convective MHD dissipative nanofluid with cross-diffusion and nonlinear velocity slip. *Numerical Heat Transfer, Part A: Applications*, 0(0), 1–19. https://doi.org/10.1080/10407782.2024.2345865.
- [39] M. Ramzan, H. Gul, J. D. Chung, S. Kadry & Y. M. Chu (2020). Significance of Hall effect and ion slip in a three-dimensional bioconvective Tangent hyperbolic nanofluid flow subject to Arrhenius activation energy. *Scientific Reports*, 10(1), Article ID: 18342. https://doi.org/10.1038/s41598-020-73365-w.
- [40] P. K. Ratha, S. Mishra, R. Tripathy & P. K. Pattnaik (2023). Analytical approach on the free convection of Buongiorno model nanofluid over a shrinking surface. In *Proceedings of The Institution of Mechanical Engineers, Part N: Journal of Nanomaterials, Nanoengineering and Nanosystems*, volume 237 pp. 83–95. England. https://doi.org/10.1177/23977914221103982.
- [41] S. K. Rawat, H. Upreti & M. Kumar (2021). Comparative study of mixed convective MHD Cuwater nanofluid flow over a cone and wedge using modified Buongiorno's model in presence of thermal radiation and chemical reaction via Cattaneo-Christov double diffusion model. *Journal of Applied and Computational Mechanics*, 7(3), 1383–1402. https://doi.org/10.22055/JACM.2020.32143.1975.
- [42] R. Razzaq, M. N. Abrar, S. Sagheer & U. Farooq (2024). Non-similar investigation of magnetohydrodynamics hybrid nanofluid flow over a porous medium with joule heating and radiative effects. *Chaos, Solitons & Fractals, 189,* Article ID: 115700. https://doi.org/10.1016/j.chaos.2024.115700.
- [43] N. A. A. Samat, N. Bachok & N. M. Arifin (2024). Boundary layer stagnation point flow and heat transfer over a nonlinear stretching/shrinking sheet in hybrid carbon nanotubes: Numerical analysis and response surface methodology under the influence of magnetohydrodynamics. *Computation*, 12(3), Article ID: 46. https://doi.org/10.3390/computation12030046.
- [44] Z. Shah, E. O. Alzahrani, W. Alghamdi & M. Z. Ullah (2020). Influences of electrical MHD and Hall current on squeezing nanofluid flow inside rotating porous plates with viscous and Joule dissipation effects. *Journal of Thermal Analysis and Calorimetry*, 140, 1215–1227. https://doi.org/10.1007/s10973-019-09176-7.
- [45] N. Shaheen, H. M. Alshehri, M. Ramzan, Z. Shah & P. Kumam (2021). Soret and Dufour effects on a Casson nanofluid flow past a deformable cylinder with variable characteristics and Arrhenius activation energy. *Scientific Reports*, 11(1), Article ID: 19282. https://doi.org/10.1038/s41598-021-98898-6.
- [46] F. Sharifat, A. Marchitto, M. S. Solari & D. Toghraie (2022). Analysis, prediction, and optimization of heat transfer coefficient and friction factor of water-nanofluid flow in shell-and-tube heat exchanger with helical baffles (using RSM). *The European Physical Journal Plus*, 137(8), Article ID: 991. https://doi.org/10.1140/epjp/s13360-022-03210-8.
- [47] B. K. Sharma, U. Khanduri, N. K. Mishra, I. Albaijan & L. M. Pérez (2023). Entropy generation optimization for the electroosmotic MHD fluid flow over the curved stenosis artery in the presence of thrombosis. *Scientific Reports*, *13*(1), Article ID: 15441. https://doi.org/10.1038/s41598-023-42540-0.

- [48] P. K. Sharma, B. K. Sharma, N. K. Mishra & H. Rajesh (2023). Impact of Arrhenius activation energy on MHD nanofluid flow past a stretching sheet with exponential heat source: A modified Buongiorno's model approach. *International Journal of Modern Physics B*, 37(32), Article ID: 2350284. https://doi.org/10.1142/S0217979223502843.
- [49] R. P. Sharma, O. Prakash, I. Rashidi, S. R. Mishra, P. S. Rao & F. Karimi (2022). Nonlinear thermal radiation and heat source effects on unsteady electrical MHD motion of nanofluid past a stretching surface with binary chemical reaction. *The European Physical Journal Plus*, 137(3), Article ID: 297. https://doi.org/10.1140/epjp/s13360-022-02359-6.
- [50] M. Turkyilmazoglu (2018). Buongiorno model in a nanofluid filled asymmetric channel fulfilling zero net particle flux at the walls. *International Journal of Heat and Mass Transfer*, 126, 974–979. https://doi.org/10.1016/j.ijheatmasstransfer.2018.05.093.
- [51] H. Zahir, K. Muhammad, F. Ali, H. A. Ghazwani & M. Hussien (2024). Numerical simulations of entropy generation and Arrhenius activation energy on peristaltic transport of Prandtl-Eyring fluid in a curved conduit. *ZAMM-Journal of Applied Mathematics and Mechanics/Zeitschrift für Angewandte Mathematik und Mechanik*, 104(4), Article ID: e202300730.